Particle collisions control stable bed configuration under weak bedload transport conditions

Thomas Christopher Ashley[1,1,1,1], Suleyman Naqshband[2,2,2,2], and Brandon McElroy[1,1,1,1]

[1]University of Wyoming
[2]University of Wageningen

November 30, 2022

Abstract

Sedimentary bed configurations that are stable under weak fluid-driven transport conditions can be divided into two groups: (1) meso-scale features that influence flow and sediment transport through roughness and drag partitioning effects ("mesoforms"), and (2) grain-scale features that can effectively be ignored at the macroscopic scale ("microforms"). In practice, these groups delineate ripples and dunes from quasi-planar bed configurations. They are thought to be separated by a transition in processes governing the relief of the bed; however, the physical mechanisms responsible for this transition are poorly understood. Previous studies suggest that planar topography is unstable when interactions between moving particles lead to stabilized bed disturbances that initiate morphodynamic pattern coarsening. This study presents a kinetic interpretation of this hypothesis in terms of parameters describing particle motion. We find that the microform/mesoform transition corresponds to a transition from rarefied to collisional transport quantified by the dimensionless ratio of particle collision frequency to particle entrainment frequency. Combined with empirical relations for bedload flux and particle travel time, theory presented herein enables prediction of bed configuration under weak bedload transport conditions.

Lower-stage plane bed topography is an outcome of rarefied, intermittent sediment transport

Thomas C. Ashley[1], **Suleyman Naqshband**[2], **Brandon McElroy**[1]

[1]Department of Geology and Geophysics, University of Wyoming, Laramie, WY
[2]Department of Environmental Sciences, Wageningen University, Wageningen, Netherlands

Key Points:

- Experiments highlight differences in particle behavior over stable and unstable planar topography.
- Stable bed configuration is controlled by a critical transition in particle behavior related to collisions between mobile particles.
- Predicted threshold of bedform initiation mirrors classic empirical stability diagrams.

Corresponding author: Thomas C. Ashley, `tashley22@gmail.com`

Abstract

Sedimentary bed configurations that are stable under weak fluid-driven transport conditions can be divided into two groups: (1) meso-scale features that influence flow and sediment transport through roughness and drag partitioning effects ("mesoforms"), and (2) grain-scale features that can effectively be ignored at the macroscopic scale ("microforms"). In practice, these groups delineate ripples and dunes from quasi-planar bed configurations. They are thought to be separated by a transition in processes governing the relief of the bed; however, the physical mechanisms responsible for this transition are poorly understood. Previous studies suggest that planar topography is unstable when interactions between moving particles lead to stabilized bed disturbances that initiate morphodynamic pattern coarsening. This study presents a kinetic interpretation of this hypothesis in terms of parameters describing particle motion. We find that the microform/mesoform transition corresponds to a critical transition in particle behavior associated with increasing importance of particle collisions. This transition also corresponds to the point where continuum-based morphodynamic models are permissible at the most unstable wavelength predicted from linear stability theory, providing a link between descriptive and mathematical theories of bedform initiation.

1 Introduction

Self-organized bedforms like ripples and dunes are essential equilibrium features of fluid driven sediment transport. They influence macroscopic flow and sediment transport through roughness and drag partitioning effects (Einstein, 1950; Engelund & Hansen, 1967; Smith & Mclean, 1977; Fredsoe, 1982; van Rijn, 1984; Wright & Parker, 2004; Best, 2005) and produce cross-bedded sedimentary architecture that can be used to interpret past flow conditions (Paola & Borgman, 1991; Leclair & Bridge, 2001; Mahon & McElroy, 2018; Leary & Ganti, 2020). However, planar topography has been observed over a narrow range of bed stresses near the threshold of motion in sand and gravel (Figure 1). Predicting the occurrence of planar topography is important from a practical standpoint because (a) grain roughness is the primary source of flow resistance (Engelund & Fredsoe, 1982), (b) sediment transport is efficient because energy is not lost to form drag (Wiberg & Smith, 1989), and (c) primary current stratification lacks recognizable cross-bedded structures (Leeder, 1980; Baas et al., 2016). Moreover, weak bedload transport conditions are common in rivers due to apparently universal constraints governing the geometry of self-formed channels (Lacey, 1930; Schumm, 1960; Ikeda et al., 1988; Dade & Friend, 1998; Eaton et al., 2004; Parker et al., 2007; Wilkerson & Parker, 2010; Métivier et al., 2017; Dunne & Jerolmack, 2018).

Despite this need, the mechanisms that control the stable bed configuration under weak bedload transport conditions are poorly understood. Studies focused on observation and documentation of morphodynamic phenomena have produced valuable descriptive theories of bedform initiation, however these are often limited in terms of their predictive power (e.g., Langbein & Leopold, 1968; P. B. Williams & Kemp, 1971; Costello, 1974; Leeder, 1980; Coleman & Melville, 1994; Coleman & Nikora, 2009). The primary theoretical approach to this problem involves modeling the fate of sinusoidal bed disturbances subject to coupled equations describing flow, sediment transport and topography (e.g., Engelund & Fredsoe, 1982; McLean, 1990; Fourrière et al., 2010; Andreotti et al., 2010; Charru et al., 2013; Bohorquez et al., 2019). This approach has clarified how simplified physical models can explain a number of commonly observed bed configurations like dunes, upper-stage plane bed, and antidunes, but most formulations predict that planar topography is unstable near the threshold of motion. One notable exception is the formulation of Andreotti et al. (2010). Their model predicts that the most stable wavelength approaches infinity at a finite excess stress in aeolian environments (Charru et al., 2013), but it is unclear whether it can explain observations of planar topography

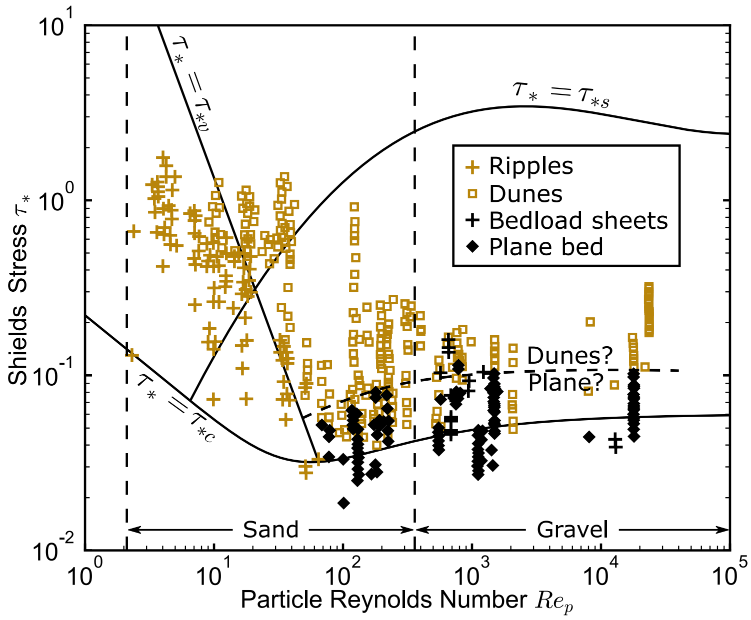

Figure 1. Shields-Parker river sedimentation diagram with empirical plane bed/dune threshold (dashed line) adapted from García (2008). The observations of bed configuration reported by Carling (1999) are plotted for comparison. Here, τ_{*v} is the viscous threshold Shields stress (García (2008), equation 2-78), τ_{*s} is the suspension threshold Shields stress (equation 2-75), and τ_{*c} is the critical Shields stress for sediment motion (equation 2-59a). Note that we distinguish between ripples and dunes according to their original classification (which may differ from modern criteria).

in rivers where the flow disturbance is expected to be transitional rather than fully turbulent.

In general, mathematical analyses have not led to a definitive explanation for the transition from stable to unstable planar topography observed in field and experimental data (Figure 1). To understand why, we look to descriptions of flow and transport processes near the threshold of motion that that have not been reconciled with modern stability theory. First, consider that a precise definition of lower-stage plane bed topography must recognize that the concept of a planar bed breaks down at scales approaching the diameters of grains. The random motion of particles driven by turbulent fluid flow causes disturbances in bed elevation (Leeder, 1980; Gyr & Schmid, 1989; Best, 1992) such that the minimum relief of a mobile bed undergoing active sediment transport is several times the nominal particle diameter (Whiting & Dietrich, 1990; Clifford et al., 1992). Notably, Martin et al. (2014) modeled evolution of grain-scale bed disturbances as a mean-reverting random walk, illustrating how a competition between disturbance growth and relaxation leads to a total bed relief that is proportional to particle diameter across a range of weak transport conditions.

Grain-scale bed disturbances may remain stable, or they may initiate pattern coarsening through nonlinear feedbacks between flow, sediment transport and topography (henceforth, "morphodynamic coarsening"). Previous studies observed the onset of significant flow separation behind disturbances (P. B. Williams & Kemp, 1971; Leeder, 1980; Best, 1996; Gyr & Kinzelbach, 2004) and defect propagation through scour-deposition waves (Raudkivi, 1963, 1966; Southard & Dingler, 1971; Costello & Southard, 1981; Gyr & Schmid, 1989; Best, 1992; Venditti et al., 2005a) when bed disturbances exceed a critical height of 2-4 particle diameters (P. B. Williams & Kemp, 1971; Leeder, 1980; Costello & Southard, 1981; Coleman & Nikora, 2009, 2011). Based on their own observations and an extensive review of previous work, Coleman and Nikora (2009) argued that bedform initiation is characterized by a two stage process. In the first stage, individual mobile particles and clusters of particles interact and create grain-scale bed disturbances when they come to rest. The second stage begins when grain-scale bed disturbances become sufficiently large to interrupt the bedload layer. We suggest that this critical disturbance height defines a transition in process regime that suitably differentiates morphodynamically-scaled "mesoforms" (e.g., ripples and dunes) from microforms like bedload sheets, particle clusters, and low-relief bedforms that scale primarily with particle diameter. Below this threshold, the bed configuration may be treated as quasi-planar for most practical purposes because (a) mobile bed roughness models already include the effect of microforms, (b) flow separation is poorly developed such that drag partitioning effects can be ignored for the purposes of predicting sediment load, and (c) preserved cross-bedding structures have a maximum thickness of several particle diameters and are likely to be indistinguishable from planar laminations in stratigraphy.

Based on this criterion, the question of bedform stability reduces to the problem of identifying the processes that control the height of grain-scale bed disturbances. Descriptive studies often report qualitative differences in collective particle behavior over stable and unstable planar topography that appear to be related to disturbance growth (Bagnold, 1935; P. B. Williams & Kemp, 1971; Costello, 1974; Coleman & Nikora, 2011). Specifically, when planar topography is stable, transport is characterized by occasional, intermittent motions of individual sediment particles. In contrast, transport over unstable planar topography is characterized by a marked increase in the overall mobility of the bed with many moving particles forming mobile patches, streaks, and hummocks (Southard & Dingler, 1971; Costello, 1974; Costello & Southard, 1981). These descriptions evoke transport thresholds that have been described in a variety of other contexts; for example, the transition from partial to full mobility observed in gravel bedded rivers (Wilcock & McArdell, 1997; Pfeiffer & Finnegan, 2018), and the transition from intermittent to continuous transport recognized in both field and numerical studies of granular motion (González et al., 2017; Martin & Kok, 2018; Pähtz et al., 2020). A number of authors also suggest that the growth of bed disturbances is connected to interactions between moving particles and congestion in the bedload phase (Bagnold, 1935; Langbein & Leopold, 1968; Costello, 1974; Coleman & Melville, 1996; Coleman & Nikora, 2009).

Our primary hypothesis is that the transition from stable to unstable planar topography is driven by a critical transport threshold associated with an increase in the importance of mobile particle interactions ("collisions"). Topographic evolution occurs through the entrainment and disentrainment of individual sediment particles; thus, we suggest that the morphodynamic importance of particle collisions may be evaluated by comparing an estimate of the particle collision frequency Z_g ($\mathrm{L}^{-2}\mathrm{T}^{-1}$) (particle collision events per second per unit bed area) with the particle entrainment frequency E_g ($\mathrm{L}^{-2}\mathrm{T}^{-1}$) (particle entrainment events per second per unit bed area). The ratio $\theta = Z_g/E_g$ (henceforth, the "collision number"), characterizes the potential for particle collisions to influence topographic change and may be interpreted as the average number of collisions from entrainment to disentrainment. When $\theta < 1$, collisions are rare and transport is dominated by isolated motions of individual particles. When $\theta > 1$, the average particle hop involves at least one collision, promoting the formation of mobile clusters of particles. Thus, we hypothesize that there is a threshold value $\theta \approx 1$ that separates transport conditions where planar topography is stable from transport conditions where planar topography is unstable.

The collision number θ has a second interpretation that is related to mathematical theories of bedform initiation. Specifically, it is an inverse Knudsen number quantifying whether continuum descriptions of transport are permissible for modeling fluctuations in the transport rate at lengthscales that are proportional to the mean particle hop distance (Furbish, 1997; Furbish et al., 2017; Rapp, 2017). This interpretation is critical because most formulations of the linear stability problem involve continuum models that express the transport rate as a function of topography and the turbulence-averaged flow field. As a result, they implicitly assume that deviations from the statistically expected transport rate can be ignored. In reality, lower-stage plane bed topography is stable under conditions where sediment transport is known to be highly intermittent (Furbish et al., 2017; Pähtz et al., 2020), exhibiting large fluctuations that are potentially consequential to the stability problem (Ancey, 2010; Ancey & Heyman, 2014). We show that continuum-based morphodynamic models break down at the most unstable wavelength predicted from linear stability theory at approximately $\theta = 1$ and hypothesize that lower-stage plane bed topography is an outcome of rarefied transport processes.

We present two proof-of-concept tests that support the hypothesized connection between particle collisions, bedload rarefaction, and lower-stage plane bed topography. First, we estimate θ from experimental observations of particle motion over stable and unstable planar topography by assuming bedload particles behave like molecules in an ideal gas. Although this assumption is not strictly valid, the basic comparison of scales may explain why numerous authors over the past century have suggested interactions between moving particles drive a shift in the balance between disturbance growth and relaxation (e.g., Bagnold, 1935; Langbein & Leopold, 1968; P. B. Williams & Kemp, 1971; Costello, 1974; Coleman & Melville, 1994; Coleman & Nikora, 2009). Results of this test reveal that the transition corresponds to a large increase in θ from $\theta < 1$ to $\theta > 1$. Second, we incorporate existing empirical formulae to predict θ as a function of hydraulic and sedimentary boundary conditions. This enables a comparison with databases reported by previous studies and leads to a predicted threshold of bedform initiation that mirrors classic empirical stability diagrams (Southard & Boguchwal, 1990; van den Berg & van Gelder, 1993; Carling, 1999). Overall, our results suggest that (a) lower-stage plane bed topography is an outcome of rarefied, intermittent transport and (b) particle collisions play a critical role in the bedform initiation process.

2 Theory

Here, we derive an expression for θ using a simplified, probabilistic model for bedload particle motion under statistically steady, uniform macroscopic transport conditions (Furbish, Haff, et al., 2012). This expression serves several purposes. First, it reveals an important connection between particle collisions and transport rarefaction. Second, it enables estimation of θ using variables that can be extracted from experimental measurements of tracer particle motion discussed in section 3. Finally, the expression for θ is combined with existing empirical transport formulae to estimate θ as a function of the macroscopic state variables that govern particle motion (section 4), enabling a direct comparison with observations of lower-stage plane bed topography and bedforms that inform classic empirical stability diagrams (Southard & Boguchwal, 1990; van den Berg & van Gelder, 1993; Carling, 1999).

Our approach is based on the assumption that inter-particle collisions may be predicted through analogy to kinetic gas theory in two dimensions (Kauzmann, 2012). We recognize that there are substantial differences between gases and bedload transport. Indeed, many studies document correlations in particle position and velocity that violate the assumptions of kinetic theory (e.g., Ancey & Heyman, 2014; Heyman et al., 2014), and mathematical models for bedload transport have been proposed that invoke analogies to other phenomena (e.g, Aussillous et al., 2013; Houssais et al., 2016; Aussillous et al., 2016). The analogy to kinetic theory is made here because it represents the simplest possible model that leads to a well-defined estimate of the collision frequency in a field of particles with randomized positions and velocities. Although there are elements of particle motion that are not captured by this analogy, we suggest that the comparison of scales outlined below provides an approximate description of a transport threshold that has been described in a variety of contexts (e.g., partial/full mobility, intermittent/continuous transport). Ultimately, every mathematical model incorporates simplifications of physical processes and must ultimately be evaluated by its ability to explain certain phenomena of interest. Below, we show that this analogy quantifies a critical transport threshold that occurs under conditions that are similar to transport thresholds described by other authors (e.g., Wilcock & McArdell, 1997; González et al., 2017; Pfeiffer & Finnegan, 2018; Pähtz et al., 2020) while providing a conceptual link between descriptive and mathematical theories of bedform initiation. We argue that the overall compatibility of this simple model for particle collisions with many disparate observations and ideas indicates that it is sufficient to describe an important underlying physical phenomenon.

Throughout this study (including above), we focus primarily on count-based descriptions of particle motion like the entrainment frequency E_g ($\mathrm{L}^{-2}\mathrm{T}^{-1}$) opposed to volumetric quantities like the entrainment rate E (LT^{-1}). Count-based (granular) quantities are denoted by the subscript g, and are related to volumetric quantities by the particle volume $V_p = \pi D^3/6$, where D (L) is the nominal particle diameter. For example, the volumetric particle activity γ (the average volume of moving particles per unit bed area) is related to the granular activity γ_g (the average number of moving particles per unit bed area) as $\gamma = V_p \gamma_g$.

In order to estimate the collision frequency for mobile bedload particles, we consider the circular projections of identical spherical particles moving in a two dimensional plane with randomized positions and velocities. In this scenario, kinetic theory predicts that the collision frequency for a single particle z_g (L^{-2}) is given by

$$z_g = 2D\gamma_g \langle|\tilde{\mathbf{u}}|\rangle. \tag{1}$$

Here, D (L) is the particle diameter and $\langle|\tilde{\mathbf{u}}|\rangle$ (LT^{-1}) is a collision velocity equal to the average magnitude of the vector difference in velocities between two randomly selected mobile particles. In an ideal gas, particles have a mean velocity of zero and follow a isotropic joint normal distribution. Integrating over the joint probability distribution of particle velocity for two independent particles leads to a collision velocity that is related to the mean particle speed $\langle|\mathbf{u}|\rangle$ as $\langle|\tilde{\mathbf{u}}|\rangle = \sqrt{2}\langle|\mathbf{u}|\rangle$.

One important difference between bedload particle motions and gas molecules is that bedload particles are advected primarily in one direction. As a result, lateral motions are small, upstream motions are rare, and downstream velocities are positively skewed. The effect of this overall behavior on the collision frequency can be estimated by substituting the isotropic joint normal distribution describing ideal gas molecule velocities with an appropriate model for the joint distribution of longitudinal and lateral bedload particle velocities. Neglecting lateral velocities and assuming longitudinal velocities follow an exponential distribution (Fathel et al., 2015; Furbish et al., 2016) leads to

$$\langle|\tilde{\mathbf{u}}|\rangle = \langle u\rangle, \tag{2}$$

where $\langle u\rangle$ is the mean longitudinal particle velocity. This simplification is verified below using measurements of tracer particle motion (section 3.6). In this case, collisions only occur because fast-moving particles overtake slow-moving particles, which is entirely consistent with descriptions of particle interactions reported by Coleman and Nikora (2009).

The collision frequency per unit bed area Z_g is computed from the collision frequency for a single particle by assuming there are γ_g identical moving particles per unit bed area, each experiencing collisions with frequency z_g. This leads to

$$Z_g = \gamma_g z_g = 2D\gamma_g^2\langle u\rangle, \tag{3}$$

Note that each collision event is counted twice (once for each particle involved in the collision) so that $\theta = Z_g/E_g$ represents the average number of collisions that a particle experiences in transit from entrainment to disentrainment.

From (3), θ may be estimated from parametric descriptions of particle motion as:

$$\theta = \frac{2D\gamma_g^2\langle u\rangle}{E_g} \tag{4}$$

Next, θ is shown to be an inverse Knudsen number (the ratio of the mean free path to a characteristic lengthscale) by substituting the following statements:

$$E_g = \frac{\gamma_g}{T_p} \tag{5}$$

$$L_x = \langle u\rangle T_p \tag{6}$$

where T_p is the mean particle travel time. These statements are valid under statistically steady, uniform macroscopic flow conditions (Furbish, Haff, et al., 2012). Finally, noting that the mean free path for particles moving in a two dimensional plane is given by $\lambda = [2D\gamma_g]^{-1}$ (Kauzmann, 2012), θ becomes

$$\theta = 2D\gamma_g\langle u\rangle T_p = L_x/\lambda. \tag{7}$$

Henceforth, we refer to conditions where $\theta < 1$ as the "rarefied regime", and $\theta > 1$ as the "collisional" regime. A schematic interpretation of this expression is presented in Figure 2.

The Knudsen number quantifies whether continuum approximations are permissible for describing fluctuations in transport rate over a specific lengthscale of interest (Furbish, 1997; Furbish et al., 2017; Rapp, 2017). Specifically, continuum models are permissible at a lengthscale L_c when $\lambda/L_c \ll 1$. Noting that the fastest growing wavelength predicted from linear stability analysis λ_i is thought to scale with a saturation length that is related to the particle hop distance L_x as a nearly constant proportion of $\lambda_i/L_x = O(10)$ in the transitional disturbance regime (Andreotti et al., 2002; Charru et al., 2013), it follows that continuum models for transport are permissible at the scale of the initial instability λ_i when $\theta \gg 0.1$. Although the failure of continuum models is gradual rather than abrupt, we argue that $\theta = O(1)$ provides a rough approximation of when this transition should occur.

In summary, the quantity θ has two interpretations. First, it is an estimate of the average number of collisions per particle hop, quantifying as transition in collective particle behavior that is qualitatively aligned with transport thresholds described in other contexts (Wilcock & McArdell, 1997; Pähtz et al., 2020). This interpretation is aligned with descriptive studies that suggest particle collisions drive a shift in the balance between granular disturbance growth and relaxation (Bagnold, 1935; Langbein & Leopold, 1968; Costello, 1974; Coleman & Melville, 1994; Coleman & Nikora, 2009, 2011). Second, it is an inverse Knudsen number quantifying the degree of rarefaction at the scale of individual particle motions. This interpretation may explain why most theoretical stability analyses fail to predict that planar topography is stable under weak bedload transport conditions: planar topography is an outcome of rarefied transport processes that occur below the resolution of continuum models that depend on the statistically expected transport rate.

With these interpretations in mind, we reiterate that (4) and (7) depend on assumptions that are not strictly valid for bedload transport. Collective entrainment effects (Ancey, 2010; Heyman et al., 2014) cause correlations in particle activity that reduce the effective distance most particles can travel before colliding with another particle relative to λ. At the same time, spatiotemporal correlations in the velocities of moving particles driven

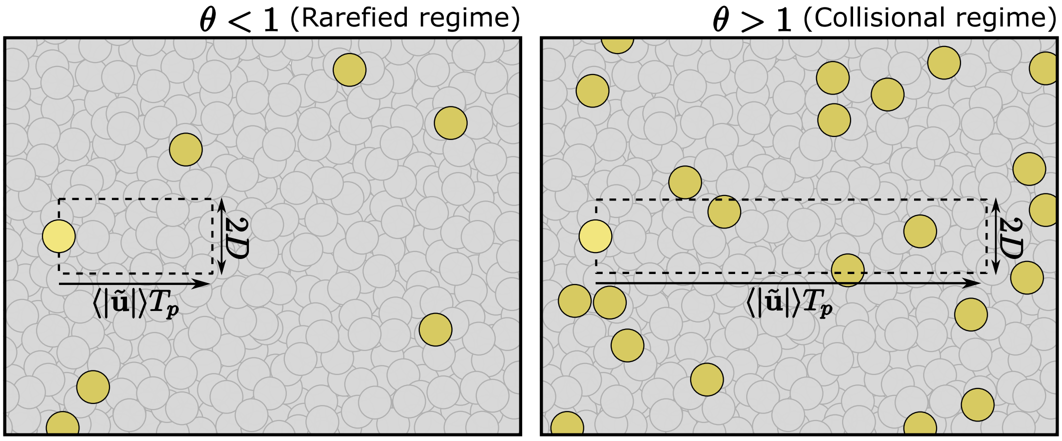

Figure 2. Schematic illustrating rarefied ($\theta < 1$) and collisional ($\theta > 1$) transport conditions. Mobile particles are shown in yellow, and immobile particles are shown in grey. A typical particle (light yellow) sweeps out a rectangle with area $2D \times \langle|\tilde{\mathbf{u}}|\rangle T_p$ during its transit from entrainment to disentrainment. The collision number θ may be interpreted as the average number of particles contained within this rectangle as a function of γ_g.

by a fluid will cause a decrease in the velocity difference between colliding particles relative to $\langle|\tilde{\mathbf{u}}|\rangle$. While both of these effects influence the true collision frequency for bedload particles, we suggest that these are second-order effects at low transport stages and that kinetic theory provides a reasonable first-order estimate that is sufficient to constrain a possible connection between bedload rarefaction, particle collisions, and bed configuration. The remainder of this paper is focused on evaluating whether theory presented here can explain observations of particle motion and bed configuration under weak bedload transport conditions.

3 Experimental Observations of Particle Motion

3.1 Description of Experiments

In this section, we investigate grain-scale transport processes under two experimental conditions characterized by (a) stable and (b) unstable planar topography. The goal of this exercise is to evaluate whether measurements of particle motion lead to estimates of θ that are compatible with our hypothesis.

Experiments were conducted in a 1.19 m wide, 14 m long flume capable of recirculating sediment and water. Flow conditions in the flume could be adjusted by varying (a) the water discharge, (b) the flow depth at the downstream end. The flume slope can also be adjusted, but the bed surface slope may vary with respect to the flume slope and is expected to adjust to an equilibrium value set by the discharge and outlet depth (Parker & Wilcock, 1993). Recognizing this, we chose to vary flow conditions by changing the water discharge while holding the outlet flow depth (12 cm) and flume slope (0.001) constant. This allowed for variation in the bed stress while maintaining a roughly constant relative submergence (the ratio of flow depth to grain size).

The bed material was composed of polystyrene particles with a geometric mean diameter of 2.1 mm and a density of 1.055 g/cm^3. The base-2 logarithmic standard deviation of the grain size distribution was 0.32 (68% of the bed material had a diameter within a factor of $2^{0.32} = 1.24$ of the geometric mean), which is narrower than most naturally-sorted sediments. The dimensionless particle Reynolds number ($Re_p = \sqrt{gRD^3}/\nu$, where

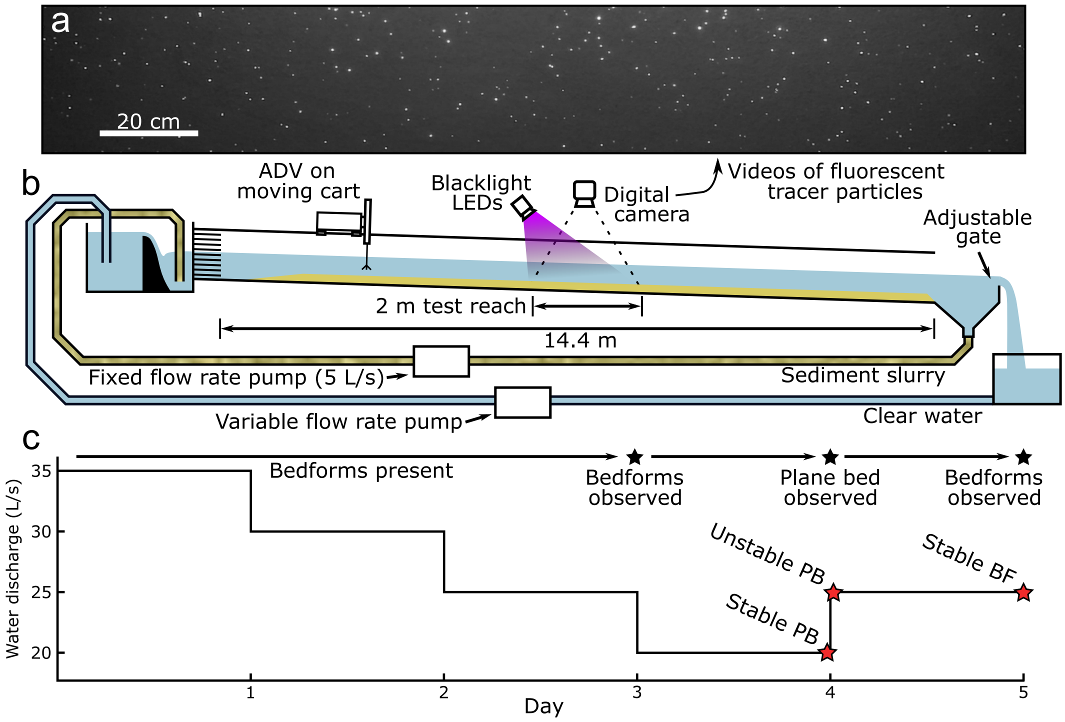

Figure 3. Schematic showing an image of fluorescent tracer particles (a), the experimental setup (b) and a timeline of the experiment (c). Red stars in the timeline indicate data collection events. Reported particle tracking data were collected over stable and unstable planar topography (labeled "Stable PB" and "Unstable PB"). Reported measurements of bedform geometry were collected over stable bedforms ("Stable BF").

R is the submerged specific gravity of the sediment, ν is the kinematic viscosity of the fluid, and g is gravitational acceleration) was approximately 70.7, which is equivalent to quartz sand ($R = 1.65$) with diameter $D = 0.68$ mm. This material covered the bed of the flume in a layer that was approximately 15 cm thick.

In order to achieve flow conditions straddling the threshold of bedform development, we initially allowed topography to equilibrate to a discharge known to produce bedload dominated bedforms (35 L/s). Then, we incrementally reduced the discharge by 5 L/s, allowing the bed to adjust for 24 hours after each reduction in discharge, until planar topography was observed. This occurred at 20 L/s. Because the planar topography was formed by the flow from an initially dune-covered bed, we are confident that it was a stable equilibrium configuration. Measurements of bed topography and particle motion were collected over equilibrium lower-stage plane topography as described in more detail below. Discharge was then increased to 25 L/s and identical measurements were immediately made over unstable plane bed topography. Finally, the bed configuration was allowed to equilibrate to the increased water discharge for roughly 24 hours to verify the presumed instability and topography was measured a third time.

Bed elevation profiles were measured using Nortek Vectrino Profiler acoustic Doppler velocimeter (ADV). The ADV was mounted to a moving cart and moved upstream and then back downstream along a 2 m longitudinal transect in the center of the flume at a speed of 3.8 cm/s. 6 scans of bed topography were collected for each experimental condition. Bed elevation profiles indicate that the total variation in bed elevation was approximately $3D$ were under stable and unstable plane bed conditions. We neglect these small bed defects in terms of their effect on macroscopic particle motion statistics. Although particle motion may exhibit conditional dependence on position with respect to bed defects, we assume that measured quantities reflect marginal distributions of particle motion (i.e. averaged over all possible positions relative to bed defects) that are relevant to the long-term evolution of bed configuration.

After the bed was allowed to equilibrate to the 25 L/s water discharge condition for 24 hours, we observed well-developed "3D" dunes (*sensu* Venditti et al., 2005b) with measured lee slopes at the angle of repose (maximum 35 degrees). Two bedform crests were visually identified in six repeat longitudinal profiles collected at 105 second intervals. These profiles covered 2 m of the bed at a spatial resolution of 1 cm. Bedform length computed as the average distance between the highest point of the crests in all six scans was 64 cm. The bedform height computed as the average height from the highest point of each crest to the lowest point before the next crest was 2.9 cm. The migration velocity estimated by averaging the displacement of the individual crests between scans was 1.4 cm/minute. Although more sophisticated methods exist for quantifying the characteristic scales of bedform topography, these basic geometric quantities are sufficient for our purposes.

3.2 Flow Conditions

The primary measure of flow strength reported here is the dimensionless bedload number $q_* = q_b/\sqrt{gRD^3}$. This is appropriate because our hypothesis leads to a predicted threshold of bedform development that may be expressed in terms of q_* (section 4). As a result, the threshold stress associated with the critical value of q_* is then estimated using empirical formulae (Brownlie, 1981; Wong & Parker, 2006; Recking, 2013). By estimating τ_* using the same approach, we quantify the relative magnitude of the experimental stress and the critical stress in a manner that is not sensitive to uncertainties associated with these empirical formulae. This exercise enables a comparison with observations reported by other authors (Figure 8), however we emphasize that precise estimates of τ_* are not critical to the hypothesis test presented in this section.

In order to provide a basic estimate of τ_* to compare our experimental conditions with other studies, we first estimate the $\tau_* - \tau_{*c}$ from q_* using the Wong & Parker (2006) bedload transport formula. Then, we estimate τ_* using a value of $\tau_{*c} = 0.032$ computed from the empirical curve of Brownlie (1984). Each of these measures of flow strength are reported in Table 1.

As mentioned previously, the equilibrium bed surface slope depends on the water discharge and outlet flow depth. In order to achieve this state, the flume must be run under fixed boundary conditions for a sufficient duration to regrade the bed to the equilibrium slope (Parker & Wilcock, 1993). Due to the relatively short durations and low transport rates in our experiments, we expect that backwater hydrodynamics influence the flow strength in the control area. This has two important implications. First, the friction slope (which scales the bed stress) is expected to deviate from the bed surface slope, water surface slope, and flume slope. Though the friction slope could be estimated from the backwater equation if the bed surface and water surface slopes are known, accurate measurement of these quantities is challenging. As a result, double-averaged (time and space) measurements of sediment load provide a more reliable proxy for flow strength than a depth slope product using any of these quantities. Second, the flow strength is expected to vary across the control area. We argue that the longitudinal changes in stress can be ignored in our experiments because the backwater length $L_{bw} = HS_b$ is much larger than the length of the control area for reasonable values of S_b, the bed surface slope. To illustrate this point, we perform a simple calculation to estimate the change in stress across the control area by extrapolating the stress gradient predicted from the backwater equation $dH/dx = (S_b - S_f)/(1 - Fr^2)$ (Chaudhry, 1993). Noting that $\tau_* = q_w/(gRC_zH)$, the backwater equation leads to

$$\frac{d\tau_*}{dx} = -\frac{\tau}{H}\frac{S_b - S_f}{1 - Fr^2}. \tag{8}$$

The change in stress $\Delta\tau_*$ across the control area length L_{tr} can be estimated by extrapolating the local gradient as $\Delta\tau_* = L_{tr}(d\tau_*/dx)$, and the fractional change in stress $|\Delta\tau_*|/\tau_*$ is given by

$$\frac{|\Delta\tau_*|}{\tau_*} = \frac{L_{tr}}{H}\frac{|S_b - S_f|}{1 - Fr^2}. \tag{9}$$

The friction slope can be estimated for both experimental conditions using the stresses estimated above and the depth measured in the control area using a ruler through the side of the flume (approximately 11 cm for both conditions) as $S_f = \tau_* RD/H$. This leads to $S_f = 5.1 \times 10^{-5}$ for the stable plane bed condition and $S_f = 8.94 \times 10^{-5}$ for the unstable plane bed condition. Though the bed surface slope is not known, we expect that it lies somewhere between the flume slope and zero. Under this assumption, the bed stress can vary by a maximum of 1.8% of its magnitude across the control area in either experiment. If it is further assumed that the bed slope was in equilibrium with the flow conditions prior to the increase in water discharge from 20 L/s to 25 L/s, ($S_b = S_f$), the estimated change in stress across the 2m long control area is 0.07 % of its magnitude for the unstable plane bed condition. Although many elements of this calculation are poorly constrained (for example, the measured flow depth in the control area), it serves to demonstrate that the basic assumption of longitudinally uniform flow is approximately valid despite the fact that backwater hydrodynamics influence the stress. We note also that observations of particle motion support this assumption: particle behavior exhibited marked qualitative differences between the two experimental conditions but did not vary noticeably in the longitudinal direction, even outside of the control area (Figure 4).

3.3 Particle Tracking

Parameters describing the kinematic properties of particle motion were extracted from manually-digitized tracer particle paths. To this end, a small fraction of the bed material was removed from the flume and coated with a thin layer of fluorescent spray paint. These particles were then added back to the flume and allowed to mix with the bed material under a range of flow conditions prior to these experiments. Illuminating the bed with a blacklight increases the contrast of tracer particles relative to other particles so that individual particles can be confidently tracked over long durations. This procedure also significantly reduces the number of particles that need to be tracked in order to obtain a representative sample of particle behavior (Naqshband et al., 2017; Ashley, Mahon, et al., 2020).

Videos of tracer particle motion were recorded using a downward facing digital camera attached to a fixed boom 2.05 m above the water surface. Because the flow velocities needed to mobilize the polystyrene particles were low relative to quartz sand, particles could be tracked through the water surface with a high degree of precision. Image rectification (which corrects for image distortion due to slight misalignment of the camera), and registration (which establishes a coordinate system in the correct units allowing for conversion from pixel position to bed position) were performed with known reference points in the flume using OpenCV (Bradski, 2000) in Python. Manual digitization of particle motions was performed using TrackMate (Tinevez et al., 2017), an open source particle tracking package for ImageJ (Schindelin et al., 2012). In order to minimize sampling bias, all tracer particle motions that occurred within the sampling window during the specified time interval were tracked. Two ten second videos comprising a total of twenty seconds of observations from each experiment were used for this study. After registration, rectification, and trimming, both videos covered a streamwise distance of 210 cm and a cross-stream distance of 99 cm. Particle behavior is sensitive to inevitable

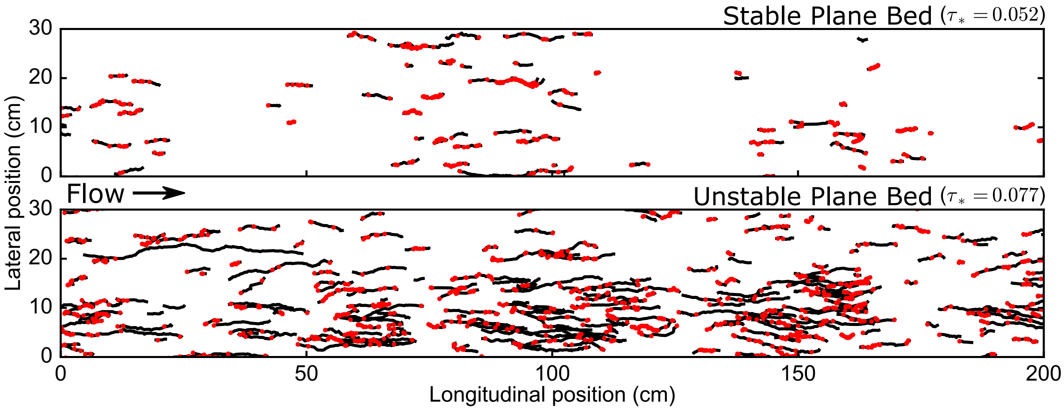

Figure 4. Tracer particle paths (black lines) and entrainment event locations (red dots) for stable and unstable plane bed conditions. Data are from the same total duration for both experiments (20 s) such that apparent differences in the densities of black lines and red dots are representative of the relative sediment loads and entrainment frequencies.

variations in shear stress that occur in the cross-stream direction (Abramian et al., 2019). For this reason, analyses reported here were performed using particle motions that occurred within a 30 cm wide, 2 m long control volume in the center of the flume corresponding to the location where shear stress was estimated from flow velocity measurements. We note that the initial phase of bedform growth began in this region and then propagated laterally to the edges of the flume. Tracked particle paths are plotted in Figure 4. Reported parametric descriptions of particle motion were computed from digitized tracer particle paths using the procedure described in 3.4.

Videos were recorded at a framerate of 30 Hz and a resolution of roughly 9.4 pixels per cm at the bed surface. Videos were downsampled to a resolution of 4.7 pixels per cm so that raster data could be stored without compression in computer memory. After rectification and registration, the length of each pixel was 2.1 mm (approximately the nominal particle diameter). Fluorescent tracer particles create a halo that illuminates adjacent pixels, and differences in pixel brightness enable robust estimation of the particle centroid location at sub-pixel resolution (Leary & Schmeeckle, 2017).

Particle tracking software records particle location with an arbitrary degree of precision depending on image magnification; thus, particles which are qualitatively identified as immobile may possess nonzero measured velocities. Following previous studies (e.g., Lajeunesse et al., 2010; Liu et al., 2019; Ashley, Mahon, et al., 2020), we employed a velocity threshold criteria to distinguish mobile and immobile particles. Velocity criteria are useful because they provide a reproducible solution to this problem, and because sensitivity analysis can easily be conducted by varying the value of the velocity threshold. For additional discussion of velocity criteria, see Ashley, Mahon, et al. (2020) and references therein. Recognizing that the motion state of certain particles is unclear, we inspected motions identified using a range of velocity thresholds and found that visual identification of particle motion corresponded to values of the velocity threshold ranging from $u_c = 0.005$ m/s to $u_c = 0.01$ m/s. Below 0.005 m/s, particles which remain in the same location for significant durations are identified as mobile, and above 0.01 m/s, particles which are clearly in motion in the bedload phase are identified as immobile. The exact values of certain computed quantities are sensitive to the specific choice of velocity threshold within this range; however, the primary findings of this work are not. Reported results were obtained using a velocity threshold of 0.007 m/s, which is approximately the geometric midpoint of the optimum range (0.005 m/s to 0.01 m/s).

In order to compute certain bulk statistics of sediment transport from tracer particle statistics, it was necessary to estimate the tracer fraction in the flume. This was accomplished by collecting a sample of material within a few centimeters of the bed surface from three locations spread across the bed after the experimental campaign was complete. Tracer particles are expected to be evenly distributed in this region due to the migration of bedforms. The total mass of the sample was 760 g. Tracer particles were separated by hand under a blacklight and then weighed. The total mass of tracer particles in the sample was 1.49 g. Thus, we estimate the tracer fraction to be 0.00196.

3.4 Methods for Computing Particle Motion Statistics From Digitized Particle Paths

3.4.1 Particle Position and Velocity

The kinematic statistics of particle motion needed to estimate θ using equation (4) were computed from digitized particle paths following Ballio et al. (2018). We consider digitized particle motions within a control volume extending from the flume bottom to the water surface projected onto a 2 dimensional plane A (Figure 4). Each particle motion is defined by a sequence of discrete measurements of particle position on the domain of longitudinal position x and lateral position y. The position of the i^{th} of m tracked particles in the t^{th} of n frames is expressed by the vector $\mathbf{x}_{i,t}$ with longitudinal and lateral components $x_{i,t}$ and $y_{i,t}$.

Particle velocities are computed by comparing subsequent positions of a particle. Measured velocities therefore represent temporal averages between the two measurements of particle position; however, the time between frames δt is sufficiently small that it may be viewed as an instantaneous velocity for our purposes. This assumption may be evaluated by comparing δt to the timescales characterizing fluctuations in particle velocity. Furbish, Ball, and Schmeeckle (2012) argue that the velocity signal must possess a fundamental harmonic with period $T = 2T_p$, implying that in the most basic sense, the mean particle travel time sets the primary scale of fluctuations in particle velocity. We estimate $T_p \gg \delta t$ for both experiments.

The velocity vector $\mathbf{u}_{i,t}$ with longitudinal and lateral components $u_{i,t}$ and $v_{i,t}$ is computed as

$$\mathbf{u}_{i,t} = \frac{\mathbf{x}_{i,t+1} - \mathbf{x}_{i,t}}{\delta t}. \tag{10}$$

Thus, the velocity attributed to frame t represents the average velocity between frame t and frame $t+1$.

3.4.2 Mean Granular Activity γ_g

The mean granular activity is computed by counting the number of active tracer particles in the control volume in each frame and averaging. This is accomplished using an Eulerian clipping function M^A to quantify whether the i^{th} tracer particle is within the control area A in the t^{th} frame:

$$M^A_{i,t} = \begin{cases} 1, & \text{if } \mathbf{x}_{i,t} \in A \\ 0, & \text{otherwise} \end{cases}. \tag{11}$$

Additionally, a velocity threshold u_c is used to define the state of motion of a particle quantified by the clipping function M^m:

$$M^m_{i,t} = \begin{cases} 1, & \text{if } |\mathbf{u}_{i,t}| \geq u_c \\ 0, & \text{otherwise} \end{cases} \tag{12}$$

Thus, the number of mobile tracer particles in the control volume in frame t is given by:

$$N^m_t = \sum_{i=1}^{m} M^m_{i,t} M^A_{i,t}. \tag{13}$$

Tracer particle positions recorded in n frames lead to $n-1$ measurements of velocity. Thus, the average number of moving tracer particles within the control volume over all frames with valid velocity measurements can be estimated as:

$$\langle N^m \rangle = \frac{1}{n-1} \sum_{t=1}^{n-1} N_t^m. \tag{14}$$

Here, angle brackets denote sample averages which provide unbiased estimates of the ensemble assuming ergodicity.

The granular activity is estimated by dividing $\langle N^m \rangle$ by the tracer particle fraction ψ and the control volume area:

$$\gamma_g = \frac{\langle N^m \rangle}{\psi A}. \tag{15}$$

Note that γ_g is an estimate of a mean, but angle brackets are dropped to simplify notation in section 2.

3.4.3 Granular Entrainment Frequency E_g

The final relevant quantity that must be estimated to compute θ with equation (7) is the entrainment frequency E_g. Entrainment and disentrainment events are defined as transitions between the mobile and immobile states and are quantified by differentiating M^m with respect to time (Ballio et al., 2018). Following this approach, we define an entrainment/disentrainment function $M^{E,D}$ as

$$M_{i,t}^{E,D} = M_{i,t}^m - M_{i,t-1}^m. \tag{16}$$

This function may take on values of 1, 0, or -1, signifying an entrainment event, no event, or a disentrainment event. In order to consider only entrainment events, values of -1 are replaced with 0, producing an entrainment function M^E. The total number of entrainment events that occur in the control area during the t^{th} frame is given by

$$N_t^E = \sum_{i=1}^{m} M_{i,t}^E M_{i,t}^A \tag{17}$$

and an estimate of the average number of entrainment events in a frame is given by

$$\langle N^E \rangle = \frac{1}{(n-2)} \sum_{t=2}^{n-1} N_t^E. \tag{18}$$

Here, $(n-2)$ is the total number of frames during which it is possible to detect entrainment events occurring in n frames. Finally, the granular entrainment frequency may be estimated by dividing the average number of entrainment events per frame by the frame duration:

$$E_g = \frac{\langle N^E \rangle}{\psi A \delta t} \tag{19}$$

The mean travel time T_p is estimated from E_g and γ_g using (5). This estimate of T_p is not biased by particles entering or leaving the control area.

3.5 Uncertainty in Estimates of q_* and θ

Uncertainty in experimental results primarily reflects uncertainty in four parameters that are estimated from data. These are (a) the tracer particle fraction ψ, (b) the average number of moving particles in the control area at any instant $\langle N^m \rangle$ (equation 14), (c) the average number of entrainment events occurring in the control area between each frame $\langle N^E \rangle$ (equation 18), and (d) the mean particle velocity $\langle u \rangle$. In order to quantify uncertainty in these parameters and propagate results through calculations of θ and

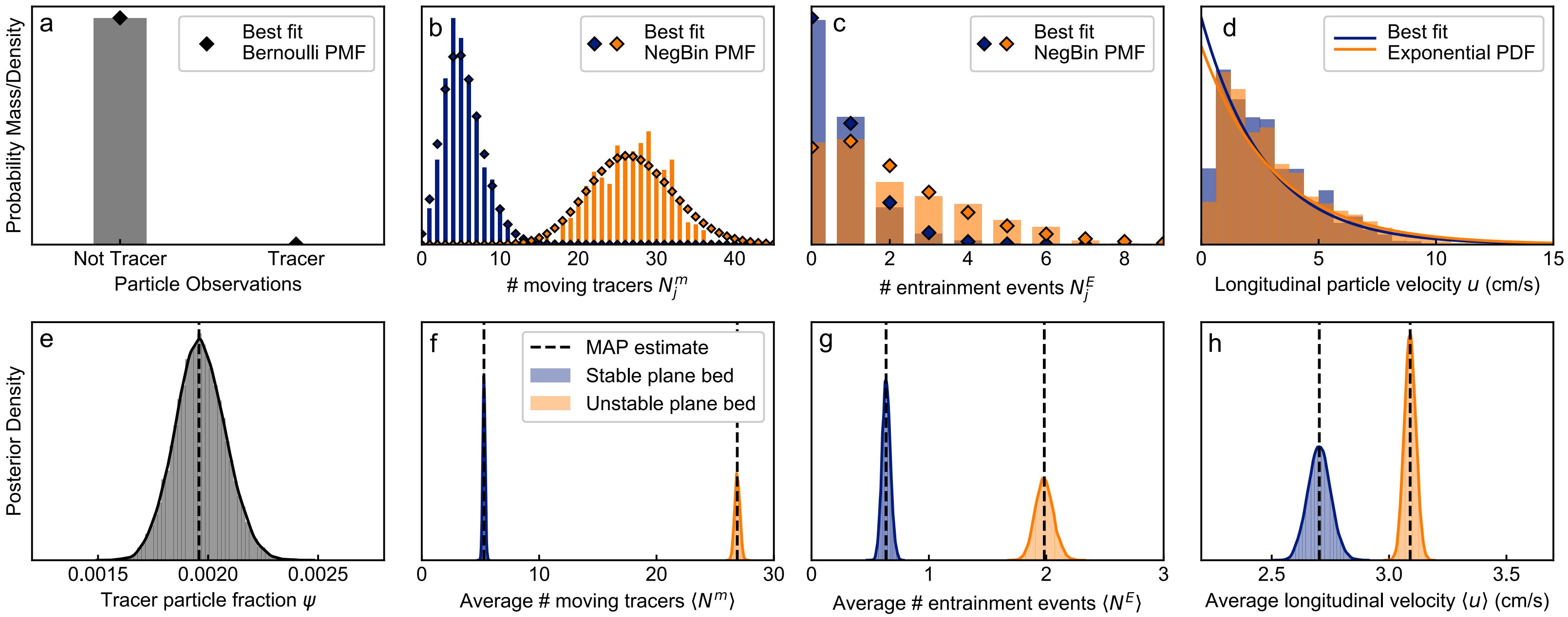

Figure 5. visualization of Bayesian uncertainty analysis. Top panels compare best-fit (Maximum a-posteriori) distributions with data. Bottom panels show maximum a-posteriori estimates and full Bayesian posterior distributions for parameters used to compute θ and q_*.

q_*, we fit theoretical distribution models to our data using Bayesian statistical techniques under the following assumptions:

- In order to estimate ψ, we assume each sampled particle may be viewed as an independent Bernoulli trial. The sample size controls the uncertainty and was estimated by dividing the sample mass by the particle mass $V_p\rho_s$, where ρ_s is the sediment density (Figure 5a).
- We assume the instantaneous number of moving particles in the control area N_t^m follows a negative binomial distribution (Ancey et al., 2008; Ancey, 2010) with parameters p and q. These parameters are related to the mean by $\langle N^m \rangle = pq/(1-p)$ (Figure 5b).
- We assume that the number of entrainment events that occur over a finite time interval between frames N_t^E follows a negative binomial distribution. Like the average number of moving particles, the number of entrainment events are expected to follow a Poisson distribution (a special case of the negative binomial distribution) if entrainment events are independent. However, we find that the Poisson distribution provides a poor fit to observations for the unstable plane bed condition, likely due to collective entrainment effects. While our use of the negative binomial distribution in this context currently lacks theoretical justification, it represents a simple way to relax the constraint that the mean is equal to the variance imposed by the Poisson distribution, leading to an improved fit. Ultimately, the estimate of the mean and the associated uncertainty is not sensitive to this choice (Figure 5c).
- We assume longitudinal particle velocities follow an exponential distribution (Furbish & Schmeeckle, 2013; Fathel et al., 2015; Furbish et al., 2016) (Figure 5d).

Probability distribution models were fit using Markov Chain Monte-Carlo (MCMC) sampling (Christensen et al., 2011) with flat priors. This approach provides a sample drawn from the posterior distribution that may be used to estimate Bayesian credible intervals and simulate predictive distributions of other quantities. Probability distributions associated with maximum a-posteriori estimates of model parameters (which are equivalent in this case to maximum likelihood estimates due to the use of flat priors) are plotted along with their full posterior distributions in Figure 5. Predictive distributions of q_* and θ (Figure 6) were simulated from MCMC samples of ψ, $\langle N^E \rangle$, $\langle N^m \rangle$, and $\langle u \rangle$ using the following expressions:

$$q_* = \frac{1}{A\sqrt{gRD^3}} \frac{\langle N^m \rangle \langle u \rangle}{\psi} \tag{20}$$

$$\theta = \frac{2D\delta t}{A} \frac{\langle N^m \rangle^2 \langle u \rangle}{\psi \langle N^E \rangle}. \tag{21}$$

These expressions reflect substitution of (15) and (19) into (4) and the activity form of the flux (Furbish, Haff, et al., 2012). Note that we do not account for uncertainty in the control area A, gravitational acceleration g, the submerged specific gravity of sediment R, the particle diameter D or the frame interval δt.

3.6 Experimental Results

Estimates of mean quantities describing tracer particle motion were computed from experimental data above using the procedure described in section 3.4. A summary of experimental conditions and results is reported in Table 3.6. Reported values of q_* and θ reflect maximum a-posteriori estimates described in section 3.5.

For the stable plane bed condition, the experimental procedure described above yielded a total of 3168 measurements of particle speed in excess of the threshold speed in the control volume belonging to 70 unique particles (Figure 4). The entrainment function

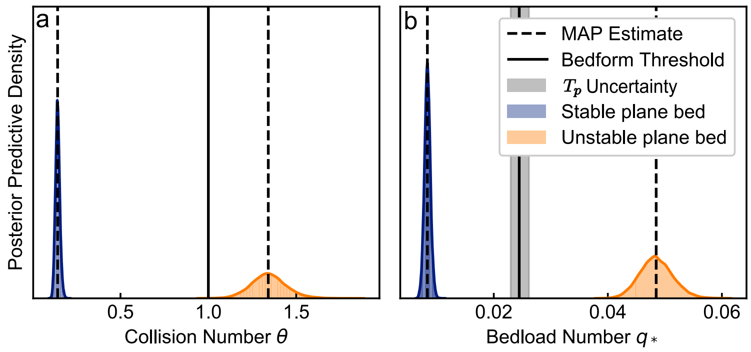

Figure 6. Results of uncertainty analysis described in section 3.5. Maximum a-posteriori estimates and posterior predictive distributions for the bedload number q_* and the collision number θ computed using Bayesian MCMC sampling. Bedform thresholds are given by $\theta = 1$ and equation (25) with $C_d = 4/3$. Grey envelope labeled "T_p Uncertainty" represents uncertainty related to the prefactor in the travel time equation reported by Lajeunesse et al. (2010) This figure represents the most appropriate estimate of uncertainty in experimental conditions relative to the hypothesized threshold of bedform initiation because none of the plotted quantities depend on an empirical model for bedload flux.

(equation 16) was used to identify a total of 798 tracer particle exchanges with the bed (entrainment and disentrainment events). The ensemble average tracer particle flux was 0.22 particles per second per meter width. This leads to a total granular flux $q_{sg} = 114$ particles per second per meter width and a bedload number $q_* = q_g V_p / \sqrt{RgD^3}$ of 0.0078. Solving the Wong and Parker (2006) bedload equation for shear velocity using the critical Shields stress predicted from Brownlie (1981) leads to $u_* = 0.74$ cm/s

For the unstable plane bed condition, experiments produced 16075 measurements of mobile particles in the control volume belonging to 238 unique particles (Figure 4). The entrainment function identified 2461 exchanges with the bed. The ensemble average tracer particle flux was 1.4 particles per second per meter width leading to a total granular flux of $q_{sg} = 688$ particles per second per meter width and a bedload number of $q_* = 0.047$. The estimated shear velocity is $u_* = 0.98$ cm/s.

Measurements of tracer particle motion also allow for verification of the simplification of the velocity distribution that leads to equation (2). We find that $\langle|\tilde{\mathbf{u}}|\rangle = 1.1\langle u\rangle$ for both experimental conditions. As a result, we argue that it is reasonable to neglect lateral and upstream motions and assume $\langle|\tilde{\mathbf{u}}|\rangle \approx \langle u\rangle$.

4 Comparison with Observations of Bed Configuration

In section 3, we estimated θ from observations of tracer particle motion to quantify collision behavior for two experimental conditions straddling the threshold of bedform development. Here, we incorporate empirical transport formulae to estimate the value of θ for observations of bed configuration that inform classic stability diagrams (Southard & Boguchwal, 1990; van den Berg & van Gelder, 1993; Carling, 1999), providing a second test of our hypothesis. As a starting point, we substitute the activity form of the average flux (Furbish, Haff, et al., 2012) in the bedload phase q_b into equation 7. The activity form of the flux is given by

$$q_b = \gamma\langle u\rangle. \tag{22}$$

Table 1. Summary of Experiments

	Stable plane bed	Unstable plane bed
Boundary Conditions		
Geometric mean particle diameter D	2.1 mm	2.1 mm
Sediment density ρ_s	1.055 g/cm^3	1.055 g/cm^3
Particle Reynolds Number Re_p	70.7	70.7
Unit water discharge q_w	0.016 m^2/s	0.021 m^2/s
Flow depth in control area h	0.11 m	0.11 m
Estimated Shields stress τ_*	0.049	0.084
Estimated shear velocity u_*	0.0074 m/s	0.0098 m/s
Results		
Granular activity γ_g	4500 m^{-2}	23,800 m^{-2}
Mean relative speed $\langle|\tilde{\mathbf{u}}|\rangle$	2.9 cm/s	3.3 cm/s
Mean longitudinal velocity $\langle u\rangle$	2.7 cm/s	3.1 cm/s
Entrainment frequency E_g	16000 m^{-2}s^{-1}	50000 m^{-2}s^{-1}
Mean travel time T_p	0.26 s	0.43 s
Granular sediment flux q_{sg}	121 m^{-1}s^{-1}	703 m^{-1}s^{-1}
Volumetric sediment flux q_s	5.88 $\times 10^{-7}$ m^2/s	3.41 $\times 10^{-6}$ m^2/s
Collision frequency Z_g	2300 m^{-2}s^{-1}	67000 m^{-2}s^{-1}
Bedload number q_*	0.0083	0.048
Mean free path λ	5.3 cm	1.0 cm
Characteristic transport length L_c	0.8 cm	1.4 cm
Collision number θ	**0.14**	**1.33**

Recall that the volumetric and granular activity are related by the particle volume as $\gamma = \gamma_g V_p$. This leads to

$$\theta = \frac{12 q_b T_p}{\pi D^2}. \tag{23}$$

Next, we consider an empirical relation for the mean particle travel time T_p. Lajeunesse et al. (2010) reviewed previous work and concluded based on physical and dimensional arguments that the mean travel time should be predicted as

$$T_p = \beta \frac{D}{\omega_s}\left(\frac{u_* - u_{*c}}{\omega_s}\right)^{\varepsilon} \tag{24}$$

where ω_s is the particle settling velocity, u_* is the shear velocity, u_{*c} is the critical shear velocity for sediment motion, and β and ε are empirical coefficients. Based on available data, they suggest that $\beta = 10.7 \pm 0.7$ and $\varepsilon = 0$, removing the dependence on u_*. We recognize that the particle travel time may possess a weak dependence on u_* despite this result. However, this does not affect the present analysis as a nonzero value of ε does not influence the trends in θ as a function of τ_* and Re_p (we return to this point below). The settling velocity is given by $\omega_s = \sqrt{4RgD/3C_d}$, where C_d is a drag coefficient. Combining equations (23) and (24) with the suggested value for β and ε leads to

$$\theta = (35.4 \pm 2.3)\sqrt{C_d} q_*. \tag{25}$$

Next, we incorporate the bedload transport formula of Recking (2013), given by

$$q_* = \frac{14\tau_*^{2.5}}{1 + (\tau_{*c}/\tau_*)^4}. \tag{26}$$

These authors propose a form for τ_{*c} that incorporates slope and sorting, however this information is not universally available for the data reported by (Carling, 1999). Instead,

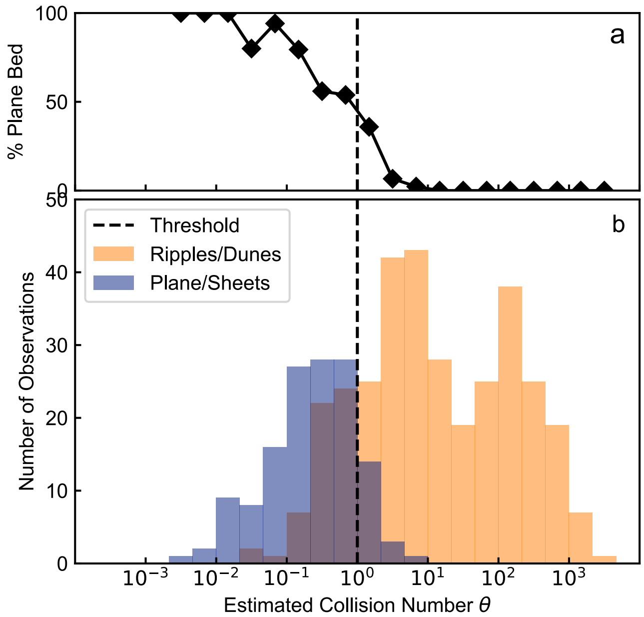

Figure 7. Plot comparing the number of observations of planar topography and bedforms at different estimated values of the collision number θ (equation 27). Panel (a) shows the percentage of observations with in a given range of θ where planar topography was observed. Panel (b) shows the total number of observations of each bed configuration. Although there is substantial overlap in observations of planar topography and bedforms, the most commonly observed bed configuration shifts from planar topography to bedforms at $\theta \approx 1$.

we consider $\tau_{*c} = f(Re_p)$ after Brownlie (1981). This approach leads to a predicted value of τ_* corresponding to $\theta = 1$ that is almost identical to the simpler formula of Wong and Parker (2006) but more appropriately characterizes small transport rates at and below the threshold of motion. Thus, we obtain

$$\theta = (35.4 \pm 2.3)\sqrt{C_d}\frac{14\tau_*^{2.5}}{1 + (\tau_{*c}/\tau_*)^4}. \tag{27}$$

Lastly, we consider $C_d = f(Re_p)$ after Ferguson and Church (2004).

Equation (27) was used to estimate θ for available observations of planar topography, bedload sheets, ripples, and dunes plotted in Figure 1. Results are plotted in Figure 7. This exercise reveals that there is a range of θ values where both planar topography and bedforms are observed. However, estimated values of θ span almost seven orders of magnitude. Planar topography is almost exclusively observed when $\theta < 0.1$ and bedforms are exclusively observed when $\theta > 10$. Within this range, there is a strong trend in the relative frequencies with which different configurations are observed with increasing θ. Critically, planar topography is more commonly observed when $\theta < 1$, while bedforms are more commonly observed when $\theta > 1$.

Figure 8 shows the stability field for planar topography implied by (27). To illustrate that our results are not sensitive to the choice of empirical bedload transport formula, the threshold of bedform initiation predicted using the (Wong & Parker, 2006) bedload equation is also plotted. Nonzero values of ε lead to a slightly different form for (27) because θ has an additional dependence on $[0.75C_d(\tau_* - \tau_{*c})]^{\varepsilon/2}$. However, this effect essentially shifts isocontours of θ up or down while preserving the overall qualitative trends. We emphasize that this model is derived assuming that bedform initiation occurs un-

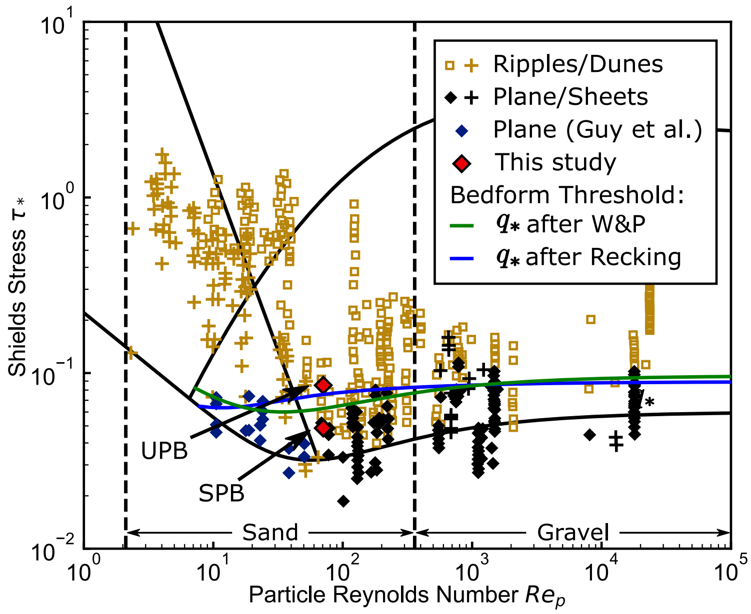

Figure 8. Shields-Parker river sedimentation diagram with theoretical plane bed/bedform transition obtained by solving equation 27 for $\theta = 1$ using two different bedload equations (Wong & Parker, 2006; Recking, 2013). Observations of planar topography and bedload sheets reported by Carling (1999) are plotted for comparison. Also plotted are observations of planar topography reported by Guy et al. (1966) that were ignored by Southard and Boguchwal (1990) and van den Berg and van Gelder (1993) in delineating classic stability fields.

der bedload-dominated transport conditions. This assumption is critical, both for the collision model described in section 2, and to scale the flux in equation (26). The stability field for lower-stage plane bed implied by (27) is not plotted above the threshold of significant suspension in Figure 8 for this reason.

Observations reported by Carling (1999) are plotted in Figure 8 for comparison with theory. This figure also includes observations of planar topography reported by Guy et al. (1966) that were ignored in subsequent studies because they are within the hydraulically smooth regime. Southard and Boguchwal (1990) asserted that these conditions would have eventually produced ripples; however, we suggest that planar topography may actually be stable indefinitely. Overall, the proposed stability field for lower-stage plane bed topography mirrors the empirical stability fields delineated using this observational data (Figure 1) but extends into the hydraulically smooth regime.

Experiments described in section 3 are also plotted in Figure 8. Note that the estimate of the stress τ_* depends on the same empirical formulae used to compute the critical value of the excess stress corresponding to $\theta = 1$. As a result, any error in the estimated value of τ_* will correspond to a commensurate error in the critical stress for bedform initiation. Uncertainty is not plotted in Figure 8 because we believe Figure 6 provides the most appropriate representation of uncertainty in experimental conditions relative to the predicted threshold of bedform initiation.

An outcome of this exercise is that the transition from rarefied to collisional transport predicted from (27) is similar to the to the transport thresholds described by other authors. For example, Pfeiffer and Finnegan (2018) describe a transition from marginal to full mobility that occurs at approximately twice the critical stress for sediment motion. Other authors have identified an important transition from intermittent to continuous transport (e.g., González et al., 2017; Pähtz et al., 2020) that is characterized by a profound reduction in the variability in the total momentum of particles over a finite bed area that also occurs at roughly twice the critical stress for sediment motion. We suggest that the alignment of these thresholds supports our use of kinetic theory for defining a critical transport rate.

4.1 Discussion

In the preceding sections, we presented two proof-of-concept tests to evaluate whether the transition from stable to unstable planar topography near the threshold of motion can be explained by a transition from rarefied to collisional transport conditions as represented in the dimensionless parameter θ. The first test (section 3) involves direct measurements of particle motion over stable and unstable planar topography, and reveals that θ increases by nearly a factor of ten, $\theta = 0.14$ to $\theta = 1.33$. The second test (section 4) involves estimating θ for observations of planar topography and bedforms across a wide range of conditions. Despite significant uncertainty in the value of θ in observational data, we find that there is a shift in the most commonly observed bed configuration at $\theta = 1$.

The dimensionless parameter θ may be interpreted as a collision number scaling the average number of particle collisions per hop, or as an inverse Knudsen number quantifying the degree of granular rarefaction at the scale of individual particle motions. We argue that these interpretations serve to unify two parallel research paradigms in bedform science. The first paradigm is focused on observation, documentation, and interpretation of phenomena and has led to conceptual models of bedform initiation that emphasize the importance of particle collisions (e.g., Coleman & Nikora, 2009). In this view, planar topography is unstable when $\theta > 1$ because particle collisions become frequent enough to shift the balance between bed disturbance growth and relaxation. In other words, when sediment transport is rarefied at the scale of individual particle motions, bed disturbance greater than one particle diameter above or below the mean bed elevation are rapidly eroded or filled in, and collisions are needed to build larger, stabilized disturbances. The second paradigm focuses on mathematical analysis of perturbations subject to the coupled equations for flow, sediment transport, and topography (e.g., Charru et al., 2013). This approach generally predicts that planar topography is unstable under weak bedload transport conditions in rivers and involves continuum descriptions of sediment transport that are only valid if the mean free path is much smaller than the lengthscale of important fluctuations. In this view, we suggest that planar topography is stable when $\theta < 1$ because the expected instability is overwhelmed by effects associated with grain-scale fluctuations in transport rate. We argue that these two interpretations provide compatible descriptions of bedform initiation.

We recognize that neither of the tests presented here provide unequivocal proof that our hypothesis is correct; building a scientific consensus would require much more data than is available at this time. Instead, we suggest that the most convincing support comes from the overall compatibility with multiple disparate lines of evidence including measurements of particle motion and observations of bed configuration reported by other authors. In particular, we emphasize that our hypothesis is consistent with a long tradition of descriptive studies that evince the importance of particle collisions while providing a link to linear stability theory.

Our work leads to several new questions. First, do correlations in particle activity and velocity influence the stable bed configuration? Our hypothesis depends on a heuristic analogy to kinetic gas theory because it is currently not clear how correlations in bedload transport influence the mean free path and collision frequency. While we argue that this approach provides a reasonable estimate of θ, it is likely that the importance of correlations varies in different settings and may play a role in governing the stable bed configuration. We note that the collision frequency for particles in a turbulent flow depends on a Stokes number quantifying the extent to which particle motions follow fluid motions. When particles perfectly follow the fluid, the collision frequency depends on the turbulent shear rate rather than the particle velocity (Saffman & Turner, 1956). Several studies have proposed models for collision frequency at intermediate Stokes numbers common in rivers (J. J. E. Williams & Crane, 1983; Sommerfeld, 2001; Oesterle & Petitjean, 1993), but these do not account for collisions with the bed that are important to bedload particle motions. Future advances in bedload particle kinetics may clarify these issues.

Another important question is why the transition from planar topography to bedforms captured in Figure 7 is gradual rather than abrupt. Overlapping observations may simply reflect the substantial uncertainties associated with empirical bedload transport formulae used to predict θ, or they may be a genuine feature of the data. Some authors have described planar beds that remain stable indefinitely unless an artificial defect is introduced (Southard & Dingler, 1971; Costello, 1974), indicating that planar topogrpahy and bedforms are metastable for a narrow range of conditions and the observed configuration. In this case, the observed condition depends on other factors like conditions at the flume and outlet or the history of the bed. If both configurations are stable for some conditions, the systematic trend in the relative frequency of observed bed configurations (Figure 7) suggests that the propensity for bedform initiation increases with θ. Alternatively, the stable bed configuration may be controlled by a third parameter that is not uniquely constrained by τ_* and Re_p. Possible candidates include the slope, Froude number, the relative particle submergence, or the particle Stokes number (which, we note, are not independent). The Stokes number in particular may be important for the reasons outlined above. The slope may also be important as it influences the value of τ_{*c} relative to that predicted by Brownlie (1981).

5 Conclusions

This paper investigates grain-scale transport processes at the onset of ripple and dune initiation. As a starting point, we recognize that the concept of planar topography breaks down at the granular scale and propose a definition of lower-stage plane bed topography that encompasses microforms with amplitudes that scale with particle diameter. This definition is appropriate because it is aligned with a hypothesized transition in the processes governing the relief of the bed. It is also aligned with practical considerations related to form roughness, drag partitioning, and preserved sedimentary structures.

Previous studies suggest that particle collisions are important during the initial phase of bedform development. We hypothesize that quasi-planar topography becomes unstable due to a critical transition in particle behavior that is related to particle collisions and propose a dimensionless parameter θ to quantify this transition. We show that θ is also an inverse Knudsen number that quantifies whether continuum models are permissible at an elementary morphodynamic lengthscale (the mean particle hop distance). Thus, an equivalent hypothesis is that planar topography is unstable when the expected morphodynamic instability is overwhelmed by granular effects.

We present two tests to evaluate whether our hypothesis is compatible with observations. First, we estimate the collision number from experimental measurements of tracer particle motion over stable and unstable planar topography. We find that the collision number is 0.14 in the stable plane bed experiment and 1.33 in the unstable plane bed experiment. Second, we incorporate empirical models for particle motion to estimate the collision numbers for an extensive database of observations bed configuration. While there is significant overlap in the observed bed configuration as a function of θ, we find that

(a) the relative frequency of observations exhibits a systematic trend as a function of θ with a shift in the most commonly observed configuration at $\theta = 1$, and (b) the condition where $\theta = 1$ mirrors classic empirical stability diagrams. These findings support the notion that particle collisions drive a shift in the balance between granular disturbance growth and relaxation and suggest that lower-stage plane bed topography is an outcome of rarefied, intermittent sediment transport.

Acknowledgments

We thank the donors of the American Chemical Society Petroleum Research Fund 54492-DNI8, the National Science Foundation (NSF) grant EAR-1632938, and the University of Wyoming School of Energy Resources for partially supporting this research. We also thank Jelle ten Harkel, Noortje Oosterhoff, and Avelon Gerritsma for assistance with experiments and particle tracking. We thank Thomas Pähtz, Stephane Bertin, two anonymous reviewers, Associate Editor Christophe Ancey, and Editor Amy East for insightful critical feedback that improved the paper. Data and code are available through Figshare (Ashley, Naqshband, & McElroy, 2020).

References

Abramian, A., Devauchelle, O., Seizilles, G., & Lajeunesse, E. (2019). Boltzmann distribution of sediment transport. *Physical Review Letters*, *123*(1). doi: 10.1103/PhysRevLett.123.014501

Ancey, C. (2010). Stochastic modeling in sediment dynamics: Exner equation for planar bed incipient bed load transport conditions. *Journal of Geophysical Research: Earth Surface*, *115*(F2), 1–21. doi: 10.1029/2009JF001260

Ancey, C., Davison, A. C., Böhm, T., Jodeau, M., & Frey, P. (2008). Entrainment and motion of coarse particles in a shallow water stream down a steep slope. *Journal of Fluid Mechanics*, *595*, 83–114. doi: 10.1017/S0022112007008774

Ancey, C., & Heyman, J. (2014). A microstructural approach to bed load transport: mean behaviour and fluctuations of particle transport rates. *Journal of Fluid Mechanics*, *744*, 129–168. doi: 10.1017/jfm.2014.74

Andreotti, B., Claudin, P., & Douady, S. (2002). Selection of dune shapes and velocities part 2: A two-dimensional modelling. *European Physical Journal B*, *28*(3), 341–352. doi: 10.1140/epjb/e2002-00237-3

Andreotti, B., Claudin, P., & Pouliquen, O. (2010). Measurements of the aeolian sand transport saturation length. *Geomorphology*, *123*(3-4), 343–348. doi: 10.1016/j.geomorph.2010.08.002

Ashley, T. C., Mahon, R. C., Naqshband, S., Leary, K. C. P., & McElroy, B. (2020). Probability distributions of particle hop distance and travel time over equilibrium mobile bedforms. *Journal of Geophysical Research: Earth Surface*, *125*(7). doi: 10.1029/2020JF005647

Ashley, T. C., Naqshband, S., & McElroy, B. J. (2020). Data and code for "Particle collisions control stable bed configuration under weak bedload transport conditions". *Figshare Dataset*. doi: 10.6084/m9.figshare.12475865.v2

Aussillous, P., Chauchat, J., Pailha, M., Médale, M., & Guazzelli, É. (2013). Investigation of the mobile granular layer in bedload transport by laminar shearing flows. *Journal of Fluid Mechanics*, *736*, 594–615. doi: 10.1017/jfm.2013.546

Aussillous, P., Zou, Z., Guazzelli, É., Yan, L., & Wyart, M. (2016). Scale-free channeling patterns near the onset of erosion of sheared granular beds. *Proceedings of the National Academy of Sciences of the United States of America*, *113*(42), 11788–11793. doi: 10.1073/pnas.1609023113

Baas, J. H., Best, J. L., & Peakall, J. (2016). Predicting bedforms and primary current stratification in cohesive mixtures of mud and sand. *Journal of the Geological Society*, *173*(1), 12–45. doi: 10.1144/jgs2015-024

Bagnold, R. A. (1935). The movement of desert sand. *Proceedings of the Royal Society of London. Series A - Mathematical and Physical Sciences*, *157*(892), 594–620. doi: 10.1098/rspa.1936.0218

Ballio, F., Pokrajac, D., Radice, A., & Hosseini Sadabadi, S. A. (2018). Lagrangian and Eulerian description of bed load transport. *Journal of Geophysical Research: Earth Surface*, *123*(2), 384–408. doi: 10.1002/2016JF004087

Best, J. L. (1992). On the entrainment of sediment and initiation of bed defects: insights from recent developments within turbulent boundary layer research. *Sedimentology*, *39*(5), 797–811. doi: 10.1111/j.1365-3091.1992.tb02154.x

Best, J. L. (1996). The fluid dynamics of small-scale alluvial bedforms. In P. A. Carling & M. R. Dawson (Eds.), *Advances in fluvial dynamics and stratigraphy* (pp. 67–125). Manchester, United Kingdom: John Wiley and Sons.

Best, J. L. (2005). The fluid dynamics of river dunes: A review and some future research directions. *Journal of Geophysical Research: Earth Surface*, *110*(F4). doi: 10.1029/2004JF000218

Bohorquez, P., Cañada-Pereira, P., Jimenez-Ruiz, P. J., & del Moral-Erencia, J. D. (2019). The fascination of a shallow-water theory for the formation of megaflood-scale dunes and antidunes. *Earth-Science Reviews*, *193*(April), 91–108. doi: 10.1016/j.earscirev.2019.03.021

Bradski, G. (2000). The OpenCV library. *Dr. Dobb's Journal of Software Tools*, *25*.

Brownlie, W. R. (1981). *Prediction of flow depth and sediment discharge in open channels* (Tech. Rep. No. 43A). Pasadena, California: W. M. Keck Laboratory of Hydraulics and Water Resources, California Institute of Technology.

Carling, P. A. (1999). Subaqueous gravel dunes. *Journal of Sedimentary Research*, *69*(3), 534–545. doi: 10.2110/jsr.69.534

Charru, F., Andreotti, B., & Claudin, P. (2013). Sand ripples and dunes. *Annual Review of Fluid Mechanics*, *45*(1), 469–493. doi: 10.1146/annurev-fluid-011212-140806

Chaudhry, M. H. (1993). *Open-Channel Flow*. Englewood Cliffs: Prentice-Hall.

Christensen, R., Johnson, W., Branscum, A., & Hanson, T. E. (2011). Simulations. In *Bayesian ideas data analysis: An introduction for scientists and statisticians* (chap. 6). Boca Raton, FL: CRC Press.

Clifford, N. J., Robert, A., & Richards, K. S. (1992). Estimation of flow resistance in gravel-bedded rivers: A physical explanation of the multiplier of roughness length. *Earth Surface Processes and Landforms*, *17*(2), 111–126. doi: 10.1002/esp.3290170202

Coleman, S. E., & Melville, B. W. (1994). Bed-form development. *Journal of Hydraulic Engineering*, *120*(5), 544–560. doi: 10.1061/(ASCE)0733-9429(1994)120:5(544)

Coleman, S. E., & Melville, B. W. (1996). Initiation of bed forms on a flat sand bed. *Journal of Hydraulic Engineering*, *122*(6), 301–309. doi: 10.1061/(asce)0733-9429(1996)122:6(301)

Coleman, S. E., & Nikora, V. I. (2009). Bed and flow dynamics leading to sediment-wave initiation. *Water Resources Research*, *45*(4), 1–12. doi: 10.1029/2007WR006741

Coleman, S. E., & Nikora, V. I. (2011). Fluvial dunes: Initiation, characterization, flow structure. *Earth Surface Processes and Landforms*, *36*(1), 39–57. doi: 10.1002/esp.2096

Costello, W. R. (1974). *Development of bed configurations in coarse sands* (Ph.D. Dissertation). Massachusetts Institute of Technology.

Costello, W. R., & Southard, J. B. (1981). Flume experiments on lower-flow-regime bed forms in coarse sand. *SEPM Journal of Sedimentary Research*, *51*(3), 849–864. doi: 10.1306/212F7DC4-2B24-11D7-8648000102C1865D

Dade, W. B., & Friend, P. F. (1998). Grain size, sediment-transport regime and channel slope in alluvial rivers. *Journal of Geology*, *106*(6), 661–675.

Dunne, K. B., & Jerolmack, D. J. (2018). Evidence of, and a proposed explanation for, bimodal transport states in alluvial rivers. *Earth Surface Dynamics*, *6*, 583–594. doi: 10.5194/esurf-6-583-2018

Eaton, B. C., Church, M., & Millar, R. G. (2004). Rational regime model of alluvial channel morphology and response. *Earth Surface Processes and Landforms*, *29*(4), 511–529. doi: 10.1002/esp.1062

Einstein, H. A. (1950). The bed-load function for sediment transportation in open channel flows. *U.S. Department of Agriculture Technical Bulletin 1026*.

Engelund, F., & Fredsoe, J. (1982). Sediment ripples and dunes. *Annual Review of Fluid Mechanics*, *14*(1), 13–37. doi: 10.1146/annurev.fl.14.010182.000305

Engelund, F., & Hansen, E. (1967). *A monograph on sediment transport in alluvial streams* (Tech. Rep.). Technical University of Denmark. doi: 10.1007/s13398-014-0173-7.2

Fathel, S., Furbish, D. J., & Schmeeckle, M. W. (2015). Experimental evidence of statistical ensemble behavior in bed load sediment transport. *Journal of Geophysical Research: Earth Surface*, *120*(11), 2298–2317. doi: 10.1002/2015JF003552

Ferguson, R. I., & Church, M. (2004). A simple universal equation for grain settling velocity. *Journal of Sedimentary Research*, *74*(6), 933–937. doi: 10.1306/051204740933

Fourrière, A., Claudin, P., & Andreotti, B. (2010). Bedforms in a turbulent stream: Formation of ripples by primary linear instability and of dunes by nonlinear pattern coarsening. *Journal of Fluid Mechanics*, *649*, 287–328. doi: 10.1017/S0022112009993466

Fredsoe, J. (1982). Shape and dimensions of stationary dunes in rivers. *Journal of the Hydraulics Division of the American Society of Civil Engineers*, *108*(8), 932–947.

Furbish, D. J. (1997). *Fluid physics in geology: An introduction to fluid motions on Earth's surface and within its crust.* New York: Oxford University Press.

Furbish, D. J., Ball, A. E., & Schmeeckle, M. W. (2012). A probabilistic description of the bed load sediment flux: 4. Fickian diffusion at low transport rates. *Journal of Geophysical Research: Earth Surface*, *117*(F3). doi: 10.1029/2012JF002356

Furbish, D. J., Fathel, S. L., Schmeeckle, M. W., Jerolmack, D. J., & Schumer, R. (2017). The elements and richness of particle diffusion during sediment transport at small timescales. *Earth Surface Processes and Landforms*, *42*(1), 214–237. doi: 10.1002/esp.4084

Furbish, D. J., Haff, P. K., Roseberry, J. C., & Schmeeckle, M. W. (2012). A probabilistic description of the bed load sediment flux: 1. Theory. *Journal of Geophysical Research: Earth Surface*, *117*(F3). doi: 10.1029/2012JF002352

Furbish, D. J., & Schmeeckle, M. W. (2013). A probabilistic derivation of the exponential-like distribution of bed load particle velocities. *Water Resources Research*, *49*(3), 1537–1551. doi: 10.1002/wrcr.20074

Furbish, D. J., Schmeeckle, M. W., Schumer, R., & Fathel, S. L. (2016). Probability distributions of bed load particle velocities, accelerations, hop distances, and travel times informed by Jaynes's principle of maximum entropy. *Journal of Geophysical Research: Earth Surface*, *121*(7), 1373–1390. doi: 10.1002/2016JF003833

García, M. H. (2008). Sediment transport and morphodynamics. In *Sedimentation engineering* (pp. 21–163). Reston, VA: American Society of Civil Engineers. doi: 10.1061/9780784408148.ch02

González, C., Richter, D. H., Bolster, D., Bateman, S., Calantoni, J., & Escauriaza, C. (2017). Characterization of bedload intermittency near the threshold of motion using a Lagrangian sediment transport model. *Environmental Fluid Mechanics*, *17*(1), 111–137. doi: 10.1007/s10652-016-9476-x

Guy, H., Simons, D. B., & Richardson, E. (1966). Summary of alluvial channel data from flume experiments, 1956-61. *U.S. Geology Survey Professional Paper 462-I*.

Gyr, A., & Kinzelbach, W. (2004). Bed forms in turbulent channel flow. *Applied Mechanics Reviews*, *57*(1), 77–93. doi: 10.1115/1.1584063

Gyr, A., & Schmid, A. (1989). The different ripple formation mechanisms. *Journal of Hydraulic Research*, *27*(1), 61–74. doi: 10.1080/00221688909499244

Heyman, J., Ma, H. B., Mettra, F., & Ancey, C. (2014). Spatial correlations in bed load transport: Evidence, importance, and modeling. *Journal of Geophysical Research F: Earth Surface*, *119*(8), 1751–1767. doi: 10.1002/2013JF003003

Houssais, M., Ortiz, C. P., Durian, D. J., & Jerolmack, D. J. (2016). Rheology of sediment transported by a laminar flow. *Physical Review E*, *94*(6), 1–10. doi: 10.1103/PhysRevE.94.062609

Ikeda, S., Parker, G., & Kimura, Y. (1988). Stable width and depth of straight gravel rivers with heterogeneous bed materials. *Water Resources Research*, *24*(5), 713–722. doi: 10.1029/WR024i005p00713

Kauzmann, W. (2012). *Kinetic theory of gases* (2nd ed.). Mineola, New York: Dover Publications, Inc.

Lacey, G. (1930). Stable channels in alluvium. *Minutes of the Proceedings of the Institution of Civil Engineers, Thomas Telford-ICE Virtual Library*, *229*, 259–292.

Lajeunesse, E., Malverti, L., & Charru, F. (2010). Bed load transport in turbulent flow at the grain scale: Experiments and modeling. *Journal of Geophysical Research: Earth Surface*, *115*(4). doi: 10.1029/2009JF001628

Langbein, W. B., & Leopold, L. B. (1968). River channel bars and dunes - Theory of kinematic waves. *U.S. Geological Survey Professional Paper 422-L.*

Leary, K. C. P., & Ganti, V. (2020). Preserved fluvial cross strata record bedform disequilibrium dynamics. *Geophysical Research Letters*, *47*(2). doi: 10.1029/2019GL085910

Leary, K. C. P., & Schmeeckle, M. W. (2017). The importance of splat events to the spatiotemporal structure of near-bed fluid velocity and bedload motion over bedforms: Laboratory experiments downstream of a backward-facing step. *Journal of Geophysical Research: Earth Surface*. doi: 10.1002/2016JF004072

Leclair, S. F., & Bridge, J. S. (2001). Quantitative interpretation of sedimentary structures formed by river dunes. *SEPM Journal of Sedimentary Research*, *71*(2), 713–716. doi: 10.1306/D4268D79-2B26-11D7-8648000102C1865D

Leeder, M. R. (1980). Discussion of the stability of lower stage plane beds and the absence of current ripples in coarse sands. *Journal of the Geological Society*, *138*(6), 753–754. doi: 10.1144/gsjgs.138.6.0753

Liu, M. X., Pelosi, A., & Guala, M. (2019). A statistical description of particle motion and rest regimes in open-channel flows under low bedload transport. *Journal of Geophysical Research: Earth Surface*, *124*(11), 2666–2688. doi: 10.1029/2019JF005140

Mahon, R. C., & McElroy, B. (2018). Indirect estimation of bedload flux from modern sand-bed rivers and ancient fluvial strata. *Geology*, *46*(7), 579–582. doi: 10.1130/G40161.1

Martin, R. L., & Kok, J. F. (2018). Distinct Thresholds for the Initiation and Cessation of Aeolian Saltation From Field Measurements. *Journal of Geophysical Research: Earth Surface*, *123*(7), 1546–1565. doi: 10.1029/2017JF004416

Martin, R. L., Purohit, P. K., & Jerolmack, D. J. (2014). Sedimentary bed evolution as a mean-reverting random walk: Implications for tracer statistics. *Geophysical Research Letters*, *41*, 6152–6159. doi: 10.1002/2014GL060525

McLean, S. R. (1990). The stability of ripples and dunes. *Earth-Science Reviews*, *29*(1-4), 131–144. doi: 10.1016/0012-8252(0)90032-Q

Métivier, F., Lajeunesse, E., & Devauchelle, O. (2017). Laboratory rivers: Lacey's law, threshold theory, and channel stability. *Earth Surface Dynamics*, *5*, 187–198. doi: 10.5194/esurf-5-187-2017

Naqshband, S., McElroy, B., & Mahon, R. C. (2017). Validating a universal model of particle transport lengths with laboratory measurements of suspended grain motions. *Water Resources Research*, *53*(5), 4106–4123. doi: 10.1002/2016WR020024

Oesterle, B., & Petitjean, A. (1993). Simulation of particle-to-particle interactions in gas solid flows. *International Journal of Multiphase Flow*, *19*(1), 199–211. doi: 10.1016/0301-9322(93)90033-Q

Pähtz, T., Clark, A. H., Valyrakis, M., & Durán, O. (2020). The physics of sediment transport initiation, cessation, and entrainment across aeolian and fluvial environments. *Reviews of Geophysics*, *58*(1). doi: 10.1029/2019RG000679

Paola, C., & Borgman, L. (1991). Reconstructing random topography from preserved stratification. *Sedimentology*, *38*(4), 553–565. doi: 10.1111/j.1365-3091.1991.tb01008.x

Parker, G., & Wilcock, P. (1993). Sediment Feed and Recirculating Flumes: Fundamental Difference. *Journal of Hydraulic Engineering*, *119*(11), 1192–1204.

Parker, G., Wilcock, P. R., Paola, C., Dietrich, W. E., & Pitlick, J. (2007). Physical basis for quasi-universal relations describing bankfull hydraulic geometry of single-thread gravel bed rivers. *Journal of Geophysical Research*, *112*(F4), F04005. doi: 10.1029/2006JF000549

Pfeiffer, A. M., & Finnegan, N. J. (2018). Regional Variation in Gravel Riverbed Mobility, Controlled by Hydrologic Regime and Sediment Supply. *Geophysical Research Letters*, *45*(7), 3097–3106. doi: 10.1002/2017GL076747

Rapp, B. E. (2017). Fluids. In *Microfluidics: Modelling, mechanics and mathematics* (pp. 243–263). Oxford, UK: Elsevier. doi: 10.1016/B978-1-4557-3141-1.50009-5

Raudkivi, A. J. (1963). Study of sediment ripple formation. *Journal of the Hydraulic Divivision of the American Society of Civil Engineers*, *89*(6), 15–34.

Raudkivi, A. J. (1966). Bed forms in alluvial channels. *Journal of Fluid Mechanics*, *26*(3), 507–514. doi: 10.1017/S0022112066001356

Recking, A. (2013). Simple Method for Calculating Reach-Averaged Bed-Load Transport. *Journal of Hydraulic Engineering*, *139*(1), 70–75. doi: 10.1061/(asce)hy.1943-7900.0000653

Saffman, P. G., & Turner, J. S. (1956). On the collision of drops in turbulent clouds. *Journal of Fluid Mechanics*, *1*(1), 16–30. doi: 10.1017/S0022112056000020

Schindelin, J., Arganda-Carreras, I., Frise, E., Kaynig, V., Longair, M., Pietzsch, T., ... Cardona, A. (2012). Fiji: an open-source platform for biological-image analysis. *Nature Methods*, *9*(7), 676–682. doi: 10.1038/nmeth.2019

Schumm, S. (1960). The shape of alluvial channels in relation to sediment type. *U.S. Geological Survey Professional Paper 352-B*.

Smith, J. D., & Mclean, S. R. (1977). Spatially averaged flow over a wavy surface. *Journal of Geophysical Research*, *82*(20). doi: 10.1029/JC082i012p01735

Sommerfeld, M. (2001). Validation of a stochastic Lagrangian modelling approach for inter-particle collisions in homogeneous isotropic turbulence. *International Journal of Multiphase Flow*, *27*(10), 1829–1858. doi: 10.1016/S0301-9322(01)00035-0

Southard, J. B., & Boguchwal, L. A. (1990). Bed configurations in steady unidirectional water flows. Part 2. Synthesis of flume data. *Journal of Sedimentary Petrology*, *60*(5), 658–679. doi: 10.1306/212f9241-2b24-11d7-8648000102c1865d

Southard, J. B., & Dingler, J. R. (1971). Flume study of ripple propagation behind mounds on flat sand beds. *Sedimentology*, *16*, 251–263. doi: 10.1111/j.1365-3091.1971.tb00230.x

Tinevez, J., Perry, N., Schindelin, J., Hoopes, G. M., Reynolds, G. D., Laplantine, E., … Eliceiri, K. W. (2017). TrackMate: An open and extensible platform for single-particle tracking. *Methods*, *115*, 80–90. doi: 10.1016/j.ymeth.2016.09.016

van den Berg, J. H., & van Gelder, A. (1993). A new bedform stability diagram, with emphasis on the transition of ripples to plane bed in flows over fine sand and silt. In *Alluvial sedimentation* (pp. 11–21). Oxford, UK: Blackwell Publishing Ltd. doi: 10.1002/9781444303995.ch2

van Rijn, L. (1984). Sediment transport, part III: Bed forms and alluvial roughness. *Journal of Hydraulic Engineering*, *110*(12), 1733–1755.

Venditti, J. G., Church, M., & Bennett, S. J. (2005b). On the transition between 2D and 3D dunes. *Sedimentology*, *52*(6), 1343–1359. doi: 10.1111/j.1365-3091.2005.00748.x

Venditti, J. G., Church, M. A., & Bennett, S. J. (2005a). Bed form initiation from a flat sand bed. *Journal of Geophysical Research: Earth Surface*, *110*(1), 1–19. doi: 10.1029/2004JF000149

Whiting, P. J., & Dietrich, W. E. (1990). Boundary shear stress and roughness over mobile alluvial beds. *Journal of Hydraulic Engineering*, *116*(12), 1495–1511. doi: 10.1061/(ASCE)0733-9429(1990)116:12(1495)

Wiberg, P. L., & Smith, J. D. (1989). Model for calculating bed load transport of sediment. *Journal of Hydraulic Engineering*, *115*(1), 101–123. doi: 10.1061/(ASCE)0733-9429(1989)115:1(101)

Wilcock, P. R., & McArdell, B. W. (1997). Partial transport of a sand/gravel sediment. *Water Resources Research*, *33*(1), 235–245. doi: 10.1029/96WR02672

Wilkerson, G. V., & Parker, G. (2010). Physical basis for quasi-universal relationships describing bankfull hydraulic geometry of sand-bed rivers. *Journal of Hydraulic Engineering*, *137*(7), 739–753. doi: 10.1061/(ASCE)HY.1943-7900.0000352

Williams, J. J. E., & Crane, R. I. (1983). Particle collision rate in turbulent flow. *International Journal of Multiphase Flow*, *9*(4), 421–435. doi: 10.1016/0301-9322(83)90098-8

Williams, P. B., & Kemp, P. H. (1971). Initiation of ripples on flat sediment beds. *Journal of the Hydraulic Divivision of the American Society of Civil Engineers*, *97*(4), 502–522.

Wong, M., & Parker, G. (2006). Reanalysis and correction of bed-load relation of Meyer-Peter and Müller using their own database. *Journal of Hydraulic Engineering*, *132*(11), 1159–1168. doi: 10.1061/(ASCE)0733-9429(2006)132:11(1159)

Wright, S. A., & Parker, G. (2004). Flow resistance and suspended load in sand-bed rivers: Simplified stratification model. *Journal of Hydraulic Engineering*, *130*(8), 796–805. doi: 10.1061/(ASCE)0733-9429(2004)130:8(796)